

Electromagnetically induced transparency in an isotopically purified $\text{Nd}^{3+}:\text{YLiF}_4$ crystal

Rinat Akhmedzhanov,^{1,2} Lev Gushchin,^{1,2} Nikolay Nizov,¹ Vladimir Nizov,¹ Dmitry Sobgayda,^{1,2} Ilya Zelensky,^{1,2} and Alexey Kalachev^{2,*}

¹*Institute of Applied Physics of the Russian Academy of Sciences, 603950 Nizhny Novgorod, Russia*

²*Zavoisky Physical-Technical Institute of the Russian Academy of Sciences, 420029 Kazan, Russia*

(Dated: March 5, 2022)

We report the first observation of electromagnetically induced transparency (EIT) in an isotopically purified $\text{Nd}^{3+}:\text{YLiF}_4$ crystal. This crystal demonstrates inhomogeneous broadening of optical transitions of about 35 MHz. EIT is observed in a symmetrical Λ -like system formed by two hyperfine sublevels of the ground state corresponding to a zero first order Zeeman (ZEFOZ) transition and a hyperfine sublevel of the excited state, which is not coupled to other ground-state sublevels. It is found that transmission of the probe field as a function of the two-photon detuning demonstrates a comb-like structure that can be attributed to superhyperfine coupling between Nd^{3+} ions and fluorine nuclei. The observed structure can be resolved only in the vicinity of the ZEFOZ point where the homogeneous linewidth of the spin transition is sufficiently small. The results pave the way for implementing solid-state quantum memories based on off-resonant Raman interaction without spectral tailoring of optical transitions.

Electromagnetically induced transparency (EIT) is a quantum interference effect which can be observed in a multilevel atomic system where resonant absorption is suppressed and a narrow transparency window is created via coherent interaction with a strong coupling field [1, 2]. Appearance of the transparency window is accompanied by strong dispersion and enhanced nonlinearity, which has led to a variety of applications including slow light propagation [3, 4], optical storage [5], precision measurements [6, 7], amplification and lasing without inversion [8], etc. In particular, EIT is a promising approach to creating optical quantum memory [9], which is a basic component required for scalable quantum computing and long-distance quantum communication [10–12]. In this respect, it is important to study EIT in materials promising for quantum storage. Among them, rare-earth-ion doped crystals at low temperature have been one of the best candidates [13] since they provide long coherence times both on optical and spin transitions, high optical density, no atomic diffusion, possibility of controlling resonant frequencies and atomic interactions by external electric and magnetic fields, etc. In particular, EIT has been extensively studied in the crystals doped by praseodymium ions [14–21], and up to now the largest EIT storage time (~ 1 min) and efficiency ($\sim 70\%$) have been demonstrated in the $\text{Pr}^{3+}:\text{Y}_2\text{SiO}_5$ crystal [20, 21]. EIT was also reported at the telecom wavelength around $1.5 \mu\text{m}$ in the same host material doped by erbium ions [22].

In this work, we present experimental results demonstrating EIT in an isotopically purified $\text{Nd}^{3+}:\text{YLiF}_4$ crystal. Neodymium doped crystals are among promising materials for quantum memory applications since they demonstrate allowed transitions at the wavelength around 850 nm, which corresponds to transparency windows both in optical fibres and atmosphere. In addition,

this wavelength is accessible for modern diode lasers and convenient for single photon detection. Odd neodymium isotopes demonstrate hyperfine structures with overall splitting in the GHz range, which is promising for storing broadband photons and microwave photons. They have long spin coherence times reaching 9 ms at cryogenic temperatures [23]. On the other hand, it has long been known that erbium and neodymium ions doped into isotopically purified YLiF_4 crystals, where only the ^7Li isotope is present, demonstrate very narrow optical transitions (~ 10 MHz) [24, 25]. Such small inhomogeneous broadening proves to be very attractive for implementing off-resonant Raman quantum memory protocols [26–30], which has recently made these crystals a subject of active research [31–35]. Since hyperfine structure of the optical transition is clearly resolved in the present material, observing EIT needs no special ensemble preparation such as spectral tailoring with anti-hole creating and optical pumping. Moreover, even superhyperfine structure can be resolved in the EIT process, which opens way for optical addressing nuclear spin states of surrounding ions and for quantum storage on the superhyperfine states as well.

Our experiments were carried out using the Y^7LiF_4 crystal (99.7% ^7Li) containing 0.005 at.% of $^{143}\text{Nd}^{3+}$ impurities (96.5% ^{143}Nd). The same material was used in [33, 36] for implementing quantum memory protocols based on atomic frequency combs. The crystal was grown by using Bridgman-Stockbarger method in an argon atmosphere of high purity (see [33, 35] for details). We started by measuring the absorption spectrum (σ polarization) of the sample on the $^4\text{I}_{9/2}(1)-^4\text{F}_{3/2}(1)$ transition (867.5 nm) at 2 K as a function of dc magnetic field directed along the crystal c axis. Two examples are shown in Fig. 1. The isotope ^{143}Nd has a nuclear spin of $I = 7/2$, while the doubly degenerate electronic states

are described by the effective electron spin $S = 1/2$. The hyperfine structure of the ground and excited states is described by the effective spin Hamiltonian

$$H = g_{\parallel}\mu_B B_z S_z + g_{\perp}\mu_B (B_x S_x + B_y S_y) + AI_z S_z + B(I_x S_x + I_y S_y) + P[I_z^2 - I(I+1)/3], \quad (1)$$

where $\mu_B = 14$ MHz/mT is the Bohr magneton, g_{\parallel} and g_{\perp} are the components of the g factor parallel and perpendicular to the c axis, B_i are the components of the external magnetic field, S_i and I_i are the electron- and nuclear-spin operators, respectively, A and B are the hyperfine parameters, and P is the quadrupole constant. The ground state parameters are known from electron paramagnetic resonance (EPR) measurements [37] (see also [25]): $A = -590$ MHz, $B = -789$ MHz, $g_{\perp} = 2.554$ and $g_{\parallel} = 1.987$. The excited state parameters can be determined from the measured optical spectra as was done in [25], which is possible due to small inhomogeneous broadening of the optical transition. In the present work, the resulting parameters for the excited state are determined to be $A = -257$ MHz, $B = -456$ MHz, and $g_{\parallel} = 0.18$, which are close to the values obtained in [25]. In both cases, the quadrupole constant is found to be negligibly small.

Considering the ground electronic state, for certain values of the external magnetic field it is expected to observe hyperfine transitions which are insensitive to the magnetic field fluctuations. Such zero first order Zeeman (ZEFOZ) transitions [38–40] can demonstrate extremely long spin coherence times [41] thereby providing the optimal conditions for quantum storage. The calculations show that the most interesting ZEFOZ transition appears under application of the longitudinal magnetic field of about 63.6 mT. In this case, the hyperfine sublevels of the ground state form an ideal symmetric Λ -scheme with a hyperfine sublevel of the excited state. To be more precise, under such a magnetic field we have the following states:

$$|8g\rangle = \frac{1}{\sqrt{2}} \left(-\left| \frac{5}{2}, \frac{1}{2} \right\rangle - \left| \frac{7}{2}, -\frac{1}{2} \right\rangle \right), \quad (2)$$

$$|10g\rangle = \frac{1}{\sqrt{2}} \left(-\left| \frac{5}{2}, \frac{1}{2} \right\rangle + \left| \frac{7}{2}, -\frac{1}{2} \right\rangle \right), \quad (3)$$

$$|9e\rangle = \left| \frac{7}{2}, \frac{1}{2} \right\rangle, \quad (4)$$

where $|me\rangle$ and $|mg\rangle$ correspond to m th sublevel of the ground (g) and excited (e) state, respectively, while $|M_I, M_S\rangle$ stands for the eigenstate of the Hamiltonian (1) with specific values of the axial component of the nuclear spin ($-7/2 \leq M_I \leq 7/2$) and of the effective electron spin ($-1/2 \leq M_S \leq 1/2$). The excited state sublevel $|9e\rangle$ is coupled only to the pair of the ground state sublevels, $|8g\rangle$ and $|10g\rangle$, by equally strong optical

transitions with σ polarization (Fig. 2). The resulting most efficient and symmetric Λ -scheme is very convenient for observing Raman interaction between the atoms and two optical fields. In particular, numerics show that it provides a large signal-to-noise ratio when single photon states are stored and reconstructed via off-resonant Raman scattering [42]. It is worth noting that in the external magnetic field the inhomogeneous broadening of the optical transitions involved is reduced to ~ 35 MHz compared to ~ 70 MHz observed in the zero field case.

The frequency of the hyperfine transition as a function

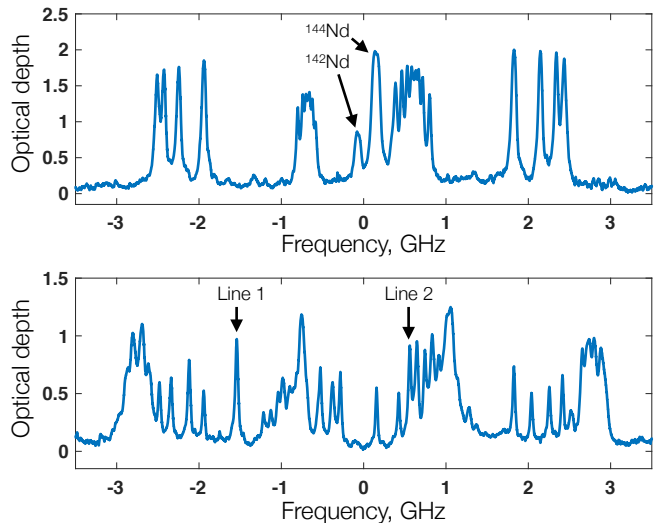


FIG. 1. Absorption spectra of the sample on the $^4I_{9/2}(1) - ^4F_{3/2}(1)$ transition in the absence of an external magnetic field (above) and in an external longitudinal magnetic field of 60.5 mT (below). The resonant lines 1 and 2 form the Λ -system that was used for EIT.

of magnetic field around the ZEFOZ point is described by the formula

$$\omega_{12} = \omega_{12}^0 + S_{2x}\Delta B_x^2 + S_{2y}\Delta B_y^2 + S_{2z}\Delta B_z^2, \quad (5)$$

where $\omega_{12}^0 \approx 2087$ MHz is the ZEFOZ transition frequency, ΔB_i is the deviation of magnetic field from the ZEFOZ point, and $S_{2i} = \partial^2 \omega_{12} / \partial B_i^2$ are the curvatures which are calculated to be $S_{2x} = S_{2y} = -52.7$ kHz/mT² and $S_{2z} = 185.3$ kHz/mT². The opposite signs of the second derivatives correspond to a saddle-type dependence (Fig. 2). At the same time, the frequencies ω_1 and ω_2 are linearly proportional to the magnetic field with the gradient $\partial \omega_{1(2)} / \partial B_i = 1.33$ MHz/mT.

The experimental setup for studying electromagnetically induced transparency is shown in Fig. 3. The emission of a single mode Ti:Sa laser (0.5 W power, 500 kHz linewidth) is split into two separate beams using a polarizing beam splitter. One of the beams is used as pump, the other as probe. The relative intensities of the two beams can be adjusted using a halfwave plate placed in

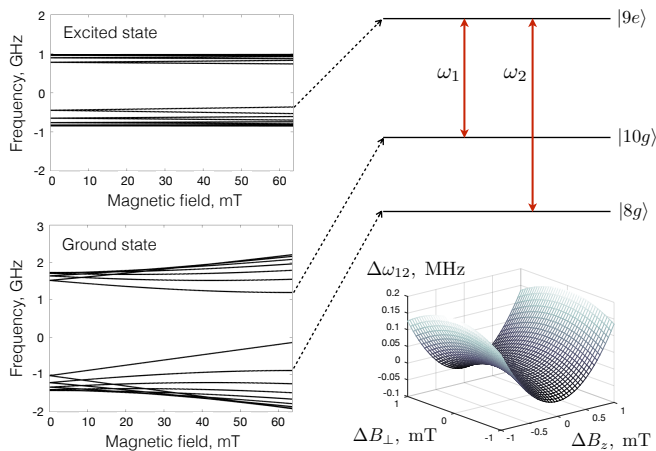


FIG. 2. Left: hyperfine structure of the electronic ground and excited states as a function of the longitudinal magnetic field. Right: hyperfine sublevels forming the identified ideal Λ -system at magnetic field of 63.6 mT (above) and the two-photon transition frequency $\Delta\omega_{12} = \omega_{12} - \omega_{12}^0$ as a function of longitudinal and transverse magnetic field deviation from the ZEFOZ point (below).

front of the beam splitter. In order to implement the required pulse sequences and frequency scans, each beam is then passed through an acousto optic modulator (AOM). The pump beam AOM (AOM₂) is set up in a single pass scheme while the probe AOM (AOM₁) is set up in the double pass scheme to avoid the beam walk during the frequency scan. The probe beam is then passed through an electro optic modulator (EOM) to create the required frequency detuning from the coupling beam. The two beams are then combined on the beam splitter and focused onto the crystal of 8 mm length that is placed inside a superconducting solenoid. The crystal and the solenoid are kept at 2 K inside a liquid helium cryostat. Both laser fields propagate along the optical c -axis and are polarized perpendicular to it (σ polarization). After the cryostat the coupling field is cut off using a polarizer (a Glan prism), while the probe field is then sent into a tunable confocal Fabry-Perot cavity for additional frequency filtering. One of the mirrors is mounted onto a piezoceramic element so that the cavity length can be controlled by external voltage. The free spectral range of the cavity was 9.4 GHz with the finesse of 11.

The described setup is meant to accomplish two tasks. The first is to control how well the coupling and probe beams spatially overlap. This is done by using the coupling beam to burn a long lived spectral hole in the inhomogeneously broadened line which is then read out using the scanned probe beam. The beams are adjusted until the depth of this hole is maximized. For this experiment, the EOM is turned off while the AOM frequencies are tuned so that the central frequencies of the two beams are the same. The second task is to select the appropriate frequency sideband of the probe beam

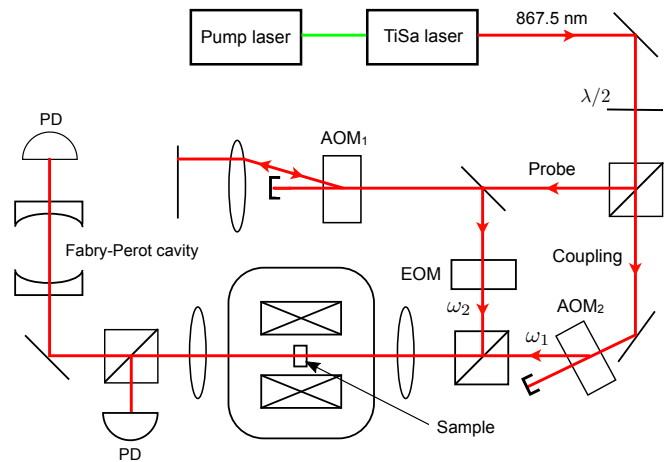


FIG. 3. Schematic of the experimental setup.

that is modulated by the EOM. This is done by measuring the absorption spectra for different sidebands. Initially, the EOM is turned off and the laser is tuned to the $|10g\rangle - |9e\rangle$ transition (Line 1 in Fig. 1). Then, the EOM is turned on and the frequency is scanned around the expected ZEFOZ transition frequency. We select one of the sidebands using the Fabry-Perot cavity and measure the absorption profile. For the correct sideband, the observed profile corresponds to the part of the spectrum around the $|8g\rangle - |9e\rangle$ transition (Line 2 in Fig. 1). For the wrong sideband, no absorption is observed. In addition, the interferometer also filters out the part of the coupling beam that is not cut off by the polarizer. In experiments the coupling field is tuned to the $|10g\rangle - |9e\rangle$ transition (Line 1) while the probe field is tuned either to the same transition for the hole burning measurements or to the $|8g\rangle - |9e\rangle$ transition (Line 2) for studying the electromagnetically induced transparency.

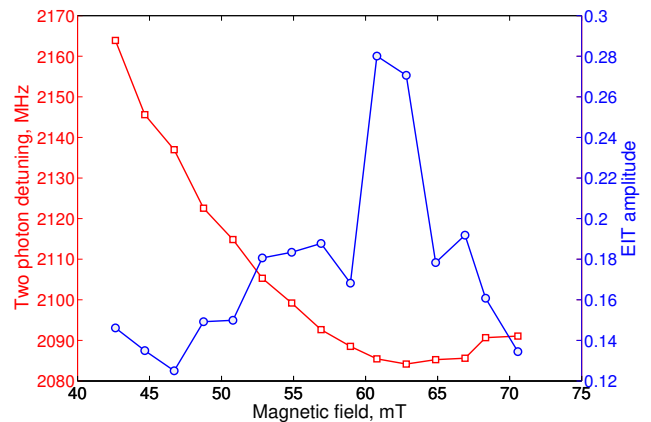


FIG. 4. The dependence of the two-photon transition frequency ω_{AB} (squares) and of the EIT amplitude (circles) on the external magnetic field in the vicinity of the ZEFOZ point. The coupling field intensity is around 50 W/cm²

EIT can be observed by comparing the intensities of the probe pulse with and without the coupling field present. When the two-photon resonance condition is satisfied, the coupling field makes the crystal more transparent for the probe pulse. The effect is described by the EIT amplitude which is defined as the ratio $(\alpha_{\text{off}} - \alpha_{\text{on}})/\alpha_{\text{off}}$, where α_{on} (α_{off}) is the resonant absorption coefficient with the coupling field tuned on (off). The experiment is performed for different values of the external magnetic field. The resulting values of the EIT amplitude and EIT resonance positions (the values of the two-photon transition frequency) are shown in Fig. 4. It can be seen that the highest transparency coincides with the location of the ZEFOZ point (the point where the two-photon transition frequency ω_{12} attains minimum as a function of the longitudinal field B_z). The dependence of ω_{12} on the magnetic field is in good agreement with the difference between the $|10g\rangle$ and $|8g\rangle$ sublevels calculated from the Hamiltonian (1).

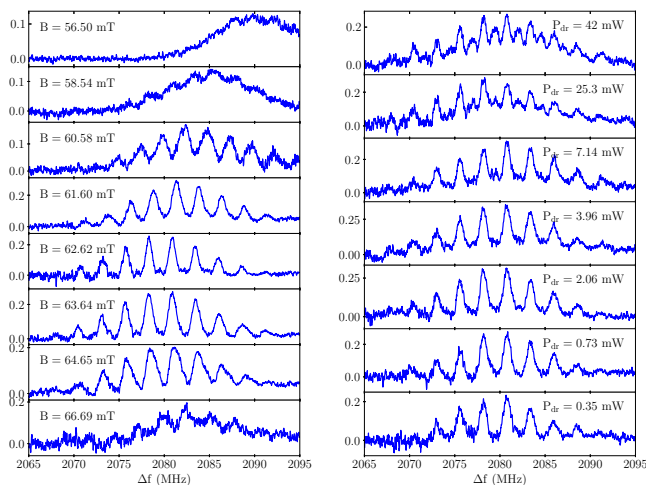


FIG. 5. Left: EIT feature profile for different values of external magnetic field. The coupling field intensity is around 7 W/cm^2 . Right: EIT feature profile for different intensities of the pump field. The crystal is located close to the beam focal point (beam waist around $100 \mu\text{m}$) and the external magnetic field is 63.6 mT . Δf is the frequency detuning of the probe field from the coupling field.

It is worth noting that the total width of the EIT feature is around 12 MHz and it does not depend on the pump intensity or the value of the external magnetic field. However, under certain conditions the internal structure of the transparency window changes. For instance, when the external magnetic field is set to the value corresponding to the ZEFOZ point, it can be seen that the EIT feature is composed of nine peaks. The peaks are separated by about 2.8 MHz and each peak is around 1 MHz wide. When the magnetic field is detuned from the ZEFOZ point, the width of each peak increases while the distance between the peaks remains the same (Fig. 5, left).

As a result, about 7 mT away from the ZEFOZ point the peaks completely overlap, forming a single 12 MHz wide EIT feature without any resolvable internal structure. In addition, an interesting effect can be observed when the pump intensity is increased (see Fig. 5, right). The resulting high pump intensities cause additional peaks to appear in the EIT feature. These peaks are located exactly between the peaks that can be observed at lower intensities.

We believe that the splitting of the EIT feature at low coupling field intensities is caused by superhyperfine interaction between the Nd^{3+} electronic spins and the neighbouring fluorine nuclear spins. Superhyperfine structure in Nd doped YLiF crystals has been previously studied using EPR in external magnetic fields both parallel and perpendicular to the crystal c -axis [43]. Similarly to this work, we observe nine separate components in the EIT feature, and the splitting between the peaks is approximately equal to the nuclear Zeeman energy of the fluorine ions (2.5 MHz for the field around 63 mT). The picture is quite similar to what is expected in the case when the superhyperfine interaction is smaller than the Zeeman energy [44]. The latter is reasonable because the expectation value of the neodymium magnetic moment in the states $|8g\rangle$ and $|10g\rangle$ is equal to zero. It is worth noting that the hole burned on the $|10g\rangle - |9e\rangle$ transition shows a similar but much less pronounced comb-like structure, which is most likely caused by the superhyperfine splitting of the excited sublevel (cf. [33]).

While the present experiment demonstrates the power of EIT as a spectroscopy method, the existence of the superhyperfine structure made it impossible to obtain transparencies close to 100% . High EIT transmission could be achieved by preparing the atomic ensemble in one of the superhyperfine states, which corresponds to polarizing fluorine nuclear spins. It has long been known that the YLiF₄ matrix is quite promising for the dynamic polarization of ^7Li and ^{19}F nuclei [45] so that higher EIT transmission seems feasible.

The blurring of the comb-like EIT structure with detuning of the magnetic field from the ZEFOZ point can be explained by increasing homogeneous broadening of the two-photon transition due to the magnetic noise. To estimate this effect, we take advantage of a simple model developed in [39] and consider Gaussian magnetic noise, which allows us to write the linewidth as

$$\Gamma(\Delta\mathbf{B}) = \Gamma_0 + \sum_{i=x,y,z} |S_{2i}| (\delta B_i) \sqrt{2(\delta B_i)^2 + 4(\Delta B_i)^2}, \quad (6)$$

where δB_i is the amplitude (variance) of the magnetic field fluctuations created by surrounding spins, $\Delta\mathbf{B} = (\Delta B_x, \Delta B_y, \Delta B_z)$ is the detuning of the external magnetic field from the ZEFOZ point, and Γ_0 is the broadening due to other effects including non-resolved overlapping of superhyperfine lines (see [44] for more details).

Then the dependence shown in Fig. 5, left is simulated quite well with the curvature values S_{2i} calculated above, $\Gamma_0 \sim 0.5$ MHz and $\delta B_i \sim 1$ mT. The latter value proves to be close the local magnetic field estimation obtained in [25]. On the other hand, such a line broadening should be accompanied by the decrease of the EIT amplitude, which indeed has been clearly observed in our experiment (Fig. 4).

To sum up, in this work we observe electromagnetically induced transparency in an isotopically pure $^{143}\text{Nd}^{3+}:\text{Y}^7\text{LiF}_4$ crystal demonstrating narrow optical transitions. We find that when the crystal is placed into an appropriate external magnetic field corresponding to the ZEFOZ point, we can resolve narrow peaks in the EIT profile. We believe that these peaks are caused by the superhyperfine splitting of the Nd^{3+} hyperfine levels in the ground electronic state. Thus, our results demonstrate that the crystal is potentially attractive for implementing Raman schemes of quantum memory involving not only hyperfine but also superhyperfine states without spectral tailoring of optical transitions.

The authors thank S.L. Korableva for the crystal growth and Pavel Bushev for useful comments and discussions. The work was supported by the Russian Science Foundation, Grant No. 14-12-00806.

* a.a.kalachev@mail.ru

- [1] S. E. Harris, *Physics Today* **50**(7), 36 (1997).
- [2] M. Fleischhauer, A. Imamoglu, and J. P. Marangos, *Rev. Mod. Phys.* **77**, 633 (2005).
- [3] L. V. Hau, S. E. Harris, Z. Dutton, and C. H. Behroozi, *Nature* **397**, 594 (1999).
- [4] D. Budker, D. F. Kimball, S. M. Rochester, and V. V. Yashchuk, *Phys. Rev. Lett.* **83**, 1767 (1999).
- [5] D. F. Phillips, A. Fleischhauer, A. Mair, R. L. Walsworth, and M. D. Lukin, *Phys. Rev. Lett.* **86**, 783 (2001).
- [6] D. Budker, W. Gawlik, D. F. Kimball, S. M. Rochester, V. V. Yashchuk, and A. Weis, *Rev. Mod. Phys.* **74**, 1153 (2002).
- [7] V. M. Acosta, K. Jensen, C. Santori, D. Budker, and R. G. Beausoleil, *Phys. Rev. Lett.* **110**, 213605 (2013).
- [8] A. S. Zibrov, M. D. Lukin, D. E. Nikonov, L. Hollberg, M. O. Scully, V. L. Velichansky, and H. G. Robinson, *Phys. Rev. Lett.* **75**, 1499 (1995).
- [9] M. Fleischhauer, and M. D. Lukin, *Phys. Rev. Lett.* **84**, 5094 (2000).
- [10] A. I. Lvovsky, B. C. Sanders, and W. Tittel, *Nature Photonics* **3**, 706 (2009).
- [11] F. Bussières, N. Sangouard, M. Afzelius, H. de Riedmatten, C. Simon, and W. Tittel, *Journal of Modern Optics* **60**, 1519 (2013).
- [12] K. Heshami, D. G. England, P. C. Humphreys, P. J. Bustard, V. M. Acosta, J. Nunn, and B. J. Sussman, *Journal of Modern Optics* **63**, 2005 (2016).
- [13] C. W. Thiel, T. Bottger, and R. L. Cone, *Journal of Luminescence* **131**, 353 (2011).
- [14] B. S. Ham, M. S. Shahriar, and P. R. Hemmer, *Opt. Lett.* **22**, 1138 (1997).
- [15] K. Ichimura, K. Yamamoto, and N. Gemma, *Phys. Rev. A* **58**, 4116 (1998).
- [16] A. V. Turukhin, V. S. Sudarshanam, M. S. Shahriar, J. A. Musser, B. S. Ham, and P. R. Hemmer, *Phys. Rev. Lett.* **88**, 023602 (2001).
- [17] J. J. Longdell, E. Fraval, M. J. Sellars, and N. B. Manson, *Phys. Rev. Lett.* **95**, 063601 (2005).
- [18] R. Akhmedzhanov, L. Gushin, E. Kuznetsova, A. Litvak, V. Yasenkov, and N. Zharova, *J. Mod. Opt.* **53**, 2449 (2006).
- [19] P. Goldner, O. Guillot-Noel, F. Beaudoux, Y. Le Du, J. Lejay, T. Chaneliere, J.-L. Le Gouet, L. Rippe, A. Amari, A. Walther, and S. Kroll, *Phys. Rev. A* **79**, 033809 (2009).
- [20] G. Heinze, C. Hubrich, and T. Halfmann, *Phys. Rev. Lett.* **111**, 033601 (2013).
- [21] D. Schraft, M. Hain, N. Lorenz, and T. Halfmann, *Phys. Rev. Lett.* **116**, 073602 (2016).
- [22] E. Baldit, K. Bencheikh, P. Monnier, S. Briau, J. A. Levenson, V. Crozatier, I. Lorgere, F. Bretenaker, J.-L. Le Gouet, O. Guillot-Noel, and P. Goldner, *Phys. Rev. B* **81**, 144303 (2010).
- [23] G. Wolfowicz, H. Maier-Flaig, R. Marino, A. Ferrier, H. Vezin, J. J. L. Morton, and P. Goldner, *Phys. Rev. Lett.* **114**, 170503 (2015).
- [24] R. M. Macfarlane, A. Cassanho, and R. S. Meltzer, *Phys. Rev. Lett.* **69**, 542 (1992).
- [25] R. M. Macfarlane, R. S. Meltzer, and B. Z. Malkin, *Phys. Rev. B* **58**, 5692 (1998).
- [26] S. A. Moiseev, and W. Tittel, *New J. Phys.* **13**, 063035 (2011).
- [27] S. A. Moiseev, *Phys. Rev. A* **88**, 012304 (2013).
- [28] X. Zhang, A. Kalachev, and O. Kocharovskaya, *Phys. Rev. A* **87**, 013811 (2013).
- [29] A. Kalachev, and O. Kocharovskaya, *Phys. Rev. A* **88**, 033846 (2013).
- [30] X. Zhang, A. Kalachev, and O. Kocharovskaya, *Phys. Rev. A* **90**, 052322 (2014).
- [31] Z.-Q. Zhou, J. Wang, C.-F. Li, and G.-C. Guo, *Scientific Reports* **3**, 2754 (2013).
- [32] R. Marino, I. Lorgere, O. Guillot-Noel, H. Vezin, A. Toncelli, M. Tonelli, J.-L. Le Gouet, and P. Goldner, *Journal of Luminescence* **169**, 478 (2016).
- [33] R. A. Akhmedzhanov, L. A. Gushchin, A. A. Kalachev, S. L. Korableva, D. A. Sobgayda, and I. V. Zelensky, *Laser Phys. Lett.* **13**, 015202 (2016).
- [34] K. I. Gerasimov, M. M. Minnegaliev, B. Z. Malkin, E. I. Baibekov, and S. A. Moiseev, *Phys. Rev. B* **94**, 054429 (2016).
- [35] N. Kukharchyk, D. Sholokhov, S. Korableva, A. Kalachev, and P. Bushev, *New J. Phys.* **20**, 023044 (2018).
- [36] R. A. Akhmedzhanov, L. A. Gushchin, A. A. Kalachev, N. A. Nizov, V. A. Sobgayda, and I. V. Zelensky, *Laser Phys. Lett.* **13**, 115203 (2016).
- [37] J. P. Sattler, and J. Nemanich, *Phys. Rev. B* **4**, 1 (1971).
- [38] E. Fraval, M. J. Sellars, and J. J. Longdell, *Phys. Rev. Lett.* **92**, 077601 (2004).
- [39] M. Lovrić, P. Glasenapp, D. Suter, B. Tumino, A. Ferrier, P. Goldner, M. Sabooni, L. Rippe, and S. Kröll, *Phys. Rev. B* **84**, 104417 (2011).
- [40] D. L. McAuslan, J. G. Bartholomew, M. J. Sellars, and

- J. J. Longdell, *Phys. Rev. A* **85**, 032339 (2012).
- [41] M. Zhong, M. P. Hedges, R. L. Ahlefeldt, J. G. Bartholomew, S. E. Beavan, S. M. Wittig, J. J. Longdell, and M. J. Sellars, *Nature* **517**, 177 (2015).
- [42] A. D. Berezhnoi, and A.A. Kalachev, *Quantum Electronics* **47**, 790 (2017).
- [43] L. K. Aminov, M. R. Gafurov, S. L. Korableva, I. N. Kurkin, and A. A. Rodionov, *Phys. Solid State* **57**, 2400 (2015).
- [44] L. K. Aminov, I. N. Kurkin, and B. Z. Malkin, *Phys. Solid State* **55**, 1343 (2013).
- [45] A. A. Antipin, B. N. Kazakov, S. L. Korableva, R. M. Rakhmatullin, Yu. K. Chirkin, and A. A. Fedii, *Soviet Physics Journal* **21**, 1187 (1978).